J. Fluid Mech. (1998), *vol.* 363, *pp.* 57–77. Printed in the United Kingdom

An experimental study of the motion of concentrated suspensions in two-dimensional channel flow. Part 2. Bidisperse systems

By M. K. LYON† AND L. G. LEAL

University of California, Santa Barbara, Department of Chemical Engineering, Santa Barbara, CA 93106, USA

(Received 13 November 1996 and in revised form 8 December 1997)

In this paper we report experimental velocity and concentration profiles for suspensions possessing a bidisperse distribution of particle size undergoing pressure-driven flow through a parallel-wall channel. In addition to the overall concentration distributions determined by implementing the modified laser Doppler velocimetry method described in Part 1 (Lyon & Leal 1998), concentration profiles for the particles of each size were measured by sampling the position of marked tracer particles across 60% of the channel gap. Non-uniform overall particle concentration distributions and blunted velocity profiles were found at bulk particle volume fractions of 0.30 and 0.40, which were equal to the monodisperse data of Part 1, within experimental uncertainty. The large-particle concentration profiles were non-uniform down to a large-particle bulk volume fraction of 0.075, while non-uniform distributions of the small particles were only found when the volume fraction of small particles in the bulk was greater than or equal to 0.20. Experiments in which at least half the suspended particulate volume was occupied by large particles revealed enrichment of the large particles in the centreline region of the channel. This size segregation was found to increase as the total number of suspended particles decreased. Finally, the data from experiments in which a uniform small-particle concentration profile was measured were compared with suspension balance model (McTigue & Jenkins 1992; Nott & Brady 1994) predictions for parameter values that corresponded only to the large particles. While close agreement with the large-particle concentration profiles was found, this comparison also reflected the fact that the small particles bring the suspension viscosity to a regime that is more sensitive to the particle concentration, rather than simply providing an increment in background viscosity to the suspending liquid.

1. Introduction

In Part 1 of this series (Lyon & Leal 1998) we reported fully developed non-uniform concentration distributions and blunted velocity profiles for monodisperse non-colloidal suspensions flowing through our parallel wall channel. Because the majority of suspensions that are processed industrially, such as rocket propellant or ceramic precursors, have a relatively broad distribution of particle size, it is important to understand the effects of polydispersity. As a significant first step, this paper reports particle velocity and concentration profiles for suspensions possessing a bimodal size distribution. Of particular interest are the relative contributions of the large and small particles to the measured particulate-phase velocity and concentration profiles.

† Present address: Department of Mechanical Engineering and Applied Mechanics, University of Michigan, Ann Arbor, MI 48109-2121, USA.

Previous studies of bidisperse suspensions have identified a number of differences in the behaviour of these systems compared to monodisperse suspensions at identical particle loadings. One example is the lower shear viscosity found for bidisperse suspensions, with the difference between bidisperse and monodisperse viscosity values increasing as either the total volume fraction of particles increases, i.e. ϕ_{bulk}, (Chong *et al.* 1971), or as the maximum attainable volume fraction is increased (Chong *et al.* 1971; Storms *et al.* 1990; Chang & Powell 1994). Another example is the lower shear-induced coefficients of diffusion reported for bidisperse suspensions by Krishnan & Leighton (1995*a*), which were also found to decrease as the maximum attainable volume fraction increased, e.g. a minimum value was observed as the fraction of total solids occupied by small particles x_s approached a value of approximately 0.3. Obviously these results for bidisperse systems under conditions in which the particles of different size remain well-mixed motivates an investigation of their behaviour for flows that are known to produce a non-uniform particle concentration distribution owing to shear-induced diffusion.

Other studies probing shear-induced migration in bidisperse suspensions have reported overall suspension behaviour similar to that found for monodisperse systems; the development of a non-uniform particle concentration distribution in which a higher concentration of particles is found to exist near the low-shear-rate region for the particular flow geometry considered (Graham *et al.* 1991; Husband *et al.* 1994; Chow *et al.* 1995; Krishnan & Leighton 1994). Also observed within this high-concentration region was an enrichment in the concentration of large particles relative to their average concentration in the suspension, which was found to occur at every size ratio of large and small particles a_l/a_s that was investigated (Husband *et al.* 1994), and was enhanced as the total number of suspended particles decreased (i.e. lower ϕ_{bulk} or x_s) (Husband *et al.* 1994; Chow *et al.* 1995). From a modelling point of view this segregation of particles by size appears to be qualitatively consistent with the particle size scaling of the shear-induced migration velocity (Leighton 1985; Leighton & Acrivos 1987; Abbott *et al.* 1991; Phillips *et al.* 1992), though it should be emphasized that a model which explicitly accounts for the interaction of particles of different size has not yet been developed.

To this point, the majority of experimental techniques used by the researchers cited above have only inferred particle size segregation for flowing bidisperse suspensions. More specifically, these methods were unable to provide concentration distributions for the particles of each size. The notable exception is the flow visualization method developed by Krishnan & Leighton (1995*b*), which enabled a complete mapping of the large- and small-particle concentration profiles within the plane of shear of a rotating belt device. In these experiments, the respective concentrations of large and small particles were found to increase and decrease in the low-shear region at the centreline of the device relative to the high-stress region at the rotating belt. Although size segregation was directly measured in these experiments, the influence of ϕ_{bulk} and x_s on size segregation has not been reported.

Based upon these results, it is apparent that a concentrated bidisperse suspension subjected to a flow field possessing a spatially varying strain rate not only produces a non-uniform overall particle concentration distribution, but also results in particle size segregation due (presumably) to the nonlinear dependence of the shear-induced migration velocity on particle size. In this work we apply the laser Doppler velocimetry (LDV) experimental technique described in Part 1 of this series to measure overall velocity and concentration profiles for the flow of bidisperse suspensions through a rectangular channel. In order to determine the flow-induced concentration distri-

butions for each of the two particle sizes within the channel gap, we utilize a microscopy method to sample the position of tracer particles within the flow. Of interest are any deviations in the overall particle velocity and concentration profiles for bidisperse suspensions compared to those previously measured for monodisperse systems. More importantly, information on the relationship between the individual particle size concentration distributions and the overall concentration and velocity profiles will be elucidated. Finally, the incorporation of two distinct methods to measure concentration profiles across the channel gap allows a direct comparison of the combined tracer particle results with the overall concentration profiles obtained via LDV.

2. Experimental method

2.1. *Materials*

The suspensions used in these experiments were similar to those used in the monodisperse experiments described in Part 1. Microspheres of poly(methyl methacrylate) (PMMA) were immersed in a suspending liquid mixture that consisted of 50% Triton X-100, 23% 1,6-dibromohexane, 13.5% UCON 75-H-90000, and 13.5% UCON 75-H-450. Particles in diameter ranges of 38–53 and 150–180 μm were recovered from polydisperse lots using stainless steel sieves (Fisher Scientific) and an electromagnetic sieve shaker (CSC Scientific). The particles were purchased from Bangs Laboratories (Terre Haute, IN) and donated by ICI Acrylics. Typical particle size distributions measured with a Coulter counter are shown in figure 1. The population average diameters for the small and large particles from these distributions were found to be 45 ± 12 μm and 155 ± 16 μm, respectively. Since the density (at 20.0 ± 0.2 °C) of the smaller particles (IC) was slightly lower than the larger ones (1.18 vs. 1.19 g cm^{-3}), the suspending fluid density was adjusted to 1.185 g cm^{-3}. Finally, microscope observations of illuminating light that was passed through a 488 nm laser line filter yielded no discernible qualitative difference in the scattered light intensity for the particles of each source when immersed in a suspending fluid of refractive index 1.4873 (at 20.0 ± 0.2 °C).

Tracer particles for the microscope-based visualization experiments were prepared by dyeing PMMA particles with RIT liquid fabric dye. The procedure used to colour them was similar to that described by Krishnan *et al.* (1996). For these experiments particles of the large and small size ranges were dyed black and orange, respectively.

2.2. *Experimental apparatus*

The LDV experimental system that was described in Part 1 was employed to measure overall particle phase velocity and concentration profiles. The flow channel utilized lucite spacers that were machined to a thickness of 0.065 in., which after being expoxied to the channel glass produced a channel gap width of 1730 μm. Data acquisition consisting of the Doppler frequency and time between consecutive Doppler bursts for particles traversing the probe volume was performed using the IFA 655 digital signal processor (TSI Inc.) and Pentium computer (Gateway) system described in Part 1.

To measure the individual concentration profiles for the particles in each size range, tracer particle positions were sampled across 60% of the channel gap utilizing the microscope arrangement shown in figure 2. This set-up consisted of a polarizing microscope (Nikon) that was placed on the LDV focusing optics side of the channel gap. The microscope was affixed to the optical table via the 90° angle bracket (Newport), adjustable height platform, and mounting post (Melles Griot) shown in the

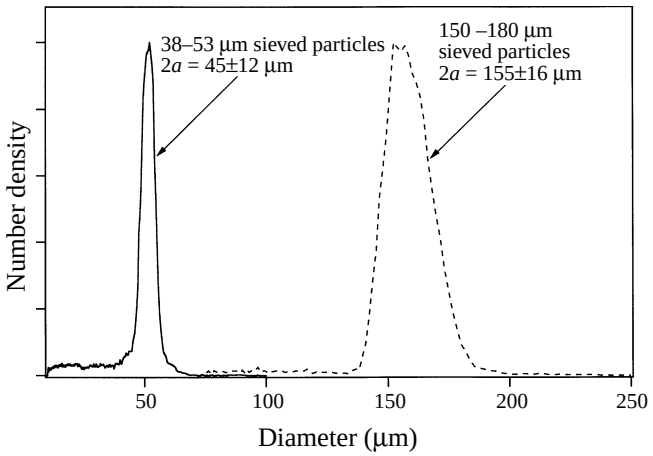

FIGURE 1. Nominal size distributions of the sieved poly(methyl methacrylate) microspheres.

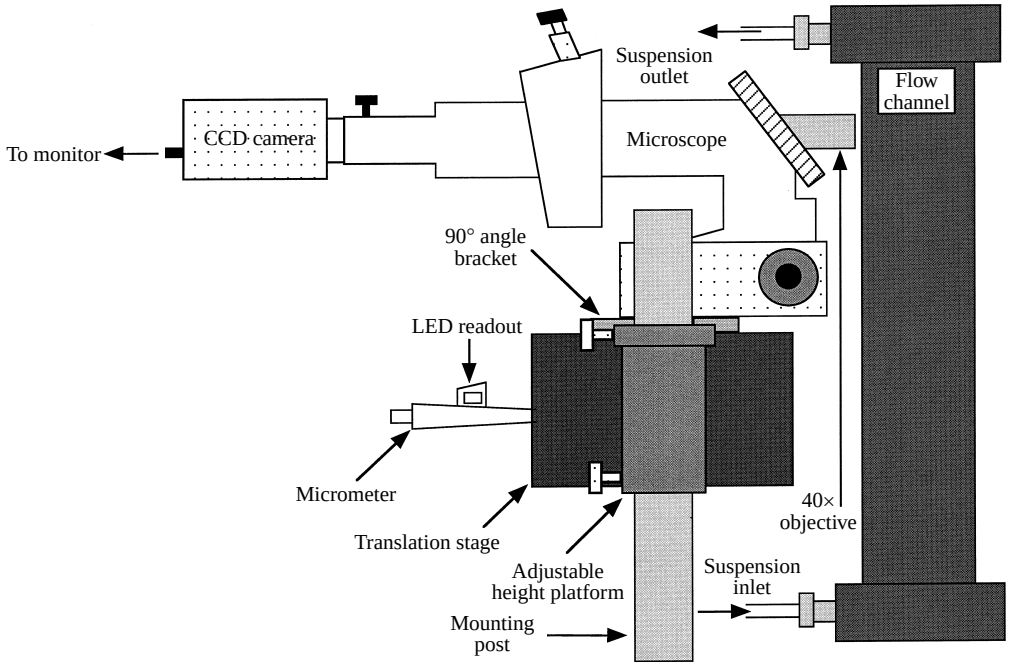

FIGURE 2. Schematic of microscope arrangement used to measure the position of tracer particles suspended within the flow.

figure. Sandwiched between these last two components was a micrometer equipped 5 in. square translation stage (Oriel) that enabled precise positioning of the microscope's objective plane within the gap region over which the tracer particle measurements were made. This micrometer had an LED readout from which the relative position of the microscope was recorded to within a tolerance of 0.0001 in.

In order to achieve a high degree of spatial resolution within the plane of shear, an objective providing a magnification of $40\times$ was incorporated. Images from the microscope were filmed with a CCD-Iris camera (Sony) that was attached to the back of the microscope, and viewed on a 12 in. colour monitor (Sony). The imaging volume provided by the entire set-up is illustrated in figure 3. The 280×280 μm area normal

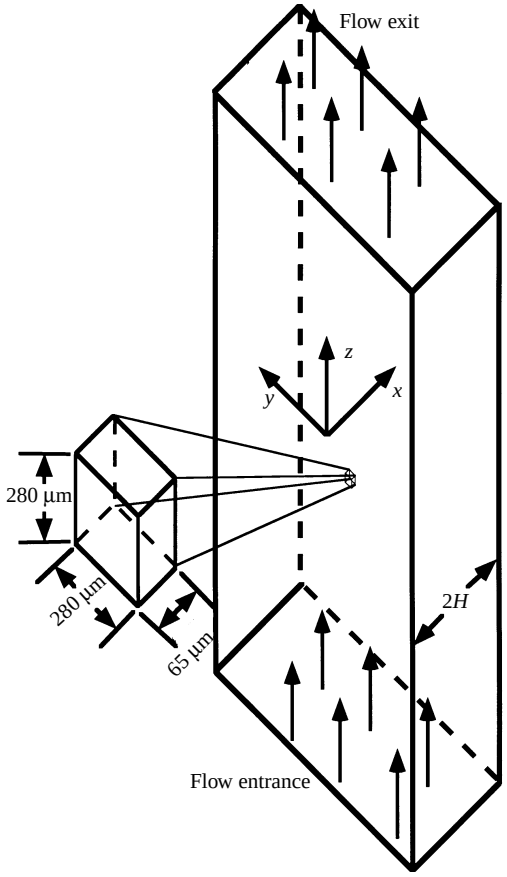

FIGURE 3. Schematic of the volume within the channel that was interrogated by the microscope.

to the plane of shear was measured with a reticule, while the depth of field shown in the figure was calculated from the uncertainty in focusing the microscope on a tracer particle. In practice the sharpness of a tracer particle image did not change appreciably over a microscope displacement that was equal to the radius of the small particles. After accounting for the fact that the microscope was translated across a medium of non-uniform index of refraction (see §3.2), this effective depth of field was found to be 65 μm.

2.3. *Experimental procedure*

The LDV optical alignment, suspension preparation, and suspension loading procedures were similar to those incorporated for the monodisperse suspensions of Part 1, and are described elsewhere (Lyon 1997). The data acquisition procedure of Part 1 was also followed, though it was modified slightly. In order to reduce potential biasing of the average velocity and concentration results due to differences in the scattered light flux from the different sized particles, the threshold voltage required by the signal processor for validation of a Doppler burst was minimized. Also, the signal processor was programmed to collect data over the entire displacement of one syringe. This latter modification enabled approximately 400 data points to be recorded near the channel wall, and 5120 frequency and inter-arrival times to be collected in the region near the channel axis.

Upon completion of the LDV experiments, data acquisition for the large and small-

particle concentration profiles was initiated. First, the microscope and flow channels were aligned in the horizontal (defined by the optical tabletop) and vertical planes to within one small-particle diameter and 0.001 in., respectively. These alignment procedures are described in Lyon (1997). The suspension was then prepared in a manner that was identical to that for the LDV experiments, except that approximately 0.1 g of tracer particles of each size range were mixed into the suspension after the index of refraction of the suspending liquid had been adjusted to its optimal value (Lyon 1997).

Tracer particle position measurements were performed over a 2 cm long section of the channel that was located 20 cm downstream from the channel entrance. After displacing one syringe (approximately 40 cm^3) of suspension through the flow system, the channel was slowly translated along its axis and the image from the microscope was monitored for suspended tracer particles lying within 1 mm of the channel wall. When a tracer particle image was intercepted, the particle was brought into sharp focus via horizontal translation of the microscope. The displacement of the microscope (relative to the inner wall) and the colour (size) of the tracer were then recorded. After achieving a total channel displacement of 2 cm another syringe of suspension was pumped through the flow system, and this procedure was repeated over the same region of the channel. For each experiment at least 3000 small and 1500 large particle positions were recorded.

3. Data reduction

3.1. *LDV local velocity and concentration measurements*

Data reduction for the LDV particle velocity and concentration profiles was identical to that discussed in Part 1 for the monodisperse experiments. Based upon the fact that the measured particle velocity profiles for the monodisperse suspensions were independent of the ratio of channel gap width to particle diameter, it was assumed that the time-average velocity profiles for the particles of each size range were identical and equal to the LDV measured result. Data reduction for the overall particle concentration profiles also neglected any particle size dependence of the probability of a particle scattering sufficient light to produce a measurable Doppler burst. The likelihood that this latter assumption is valid was maximized by instituting a minimal threshold voltage setting on the signal processor. From the standpoint of the LDV method, therefore, the bidisperse suspensions were treated in the same manner as a monodisperse system with regard to the measurement of the particulate-phase velocity and concentration distributions.

3.2. *Tracer particle local concentration measurements*

Prior to reducing the tracer-particle position data into concentration profiles for the two individual particle sizes, it was necessary to calculate the actual channel position of each tracer particle. Because particle positions were measured by translating the microscope across a medium of non-uniform index of refraction, the particle positions had to be corrected in order to account for this inhomogeneity of refractive index. A ray tracing analysis (Lyon 1997) found that the actual position of a tracer particle within the channel is proportional to the horizontal displacement of the microscope $x_{measured}$,

$$x_{actual} = x_{measured}(\tan\theta_a/\tan\theta_s), \tag{1}$$

where θ_a and θ_s are the propagation angles for light rays in air and the suspension, respectively. To determine the value of $\tan\theta_a/\tan\theta_s$ (which is greater than unity since

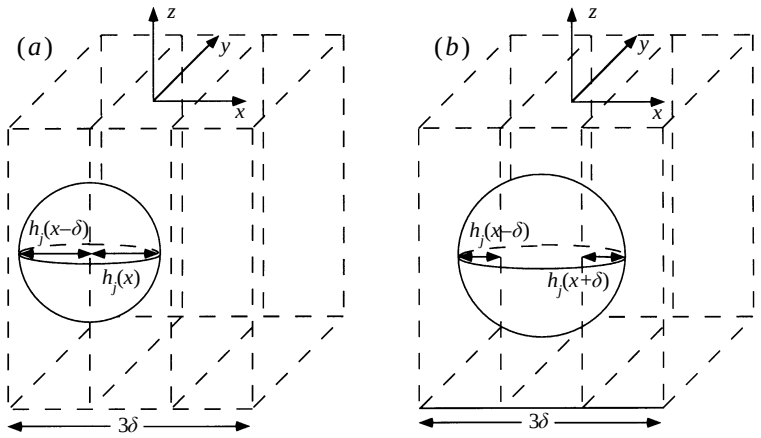

FIGURE 4. Schematic illustrating the segment length(s) of a particle that (*a*) partially overlaps, and (*b*) completely overlaps a bin.

the index of refraction of the suspension is larger than that of air), the width of the channel gap was measured while it was empty (i.e. $\theta_s = \theta_a$), and then a second time after it was filled with suspending liquid. These measurements yielded $\tan\theta_a/\tan\theta_s = 1.46$, which was utilized for calculating x_{actual} from (1).

The relative concentration distributions for the large and small particles were determined from the actual tracer particle positions at ten spatial positions spanning 56% of the channel gap by discretizing this region into ten equally spaced bins. Since all the bins have the same total volume, the relative volume fraction of particles of a particular size range (i.e. large or small) within each bin can be written as

$$\phi_i(x) \propto \begin{bmatrix}\text{total volume of particles of size range } i \\ \text{occupying the bin centred about } x\end{bmatrix}. \tag{2}$$

Owing to the inherent turbidity of the suspensions at the concentrations of interest, it was not possible to optically measure the position of every suspended particle within a particular bin. Instead, as indicated earlier, dyed tracer particles were introduced that were otherwise identical to the refractive-index-matched particles. Their relative concentrations were determined by calculating their total volume within each bin. Since the probability of a suspended particle being a tracer is governed by Poisson statistics, (2) can be expressed in terms of the total volume of tracer particles of size range i measured within the bin centred at x,

$$\phi_i(x) \propto V_{t_i}(x). \tag{3}$$

The right-hand side of (3) was determined from the approximate 1500 large and 3000 small measured tracer particle positions.

To compute V_{t_i} it was necessary to recognize that it consists of the volume of tracer particles which lie completely within a particular bin, as well as the total volume of tracer particle segments that overlap that bin. As a result of the bin spacing, the former is applicable only to the small tracer particles,

$$\begin{bmatrix}\text{total volume of small tracer} \\ \text{particles lying completely} \\ \text{within the bin centred} \\ \text{about } x\end{bmatrix} = N_i(x)\, V_s, \tag{4}$$

where $N_i(x)$ is the number of small tracer particles measured in the bin centred about x, and V_s is the average volume of the small tracers.

The particulate volume within each bin due to overlapping particles depends upon whether the particle partially or completely overlaps the bin. In the case of partial overlap, the tracer particle volume lying within the bin is given by (Beyer 1984),

$$\begin{array}{l}\text{tracer particle volume}\\ \text{due to partial overlap}\\ \text{of the bin centred at } x\end{array} = \sum_{j=1}^{N_p(x)} \frac{\pi}{3} h_j^2(x)(3a_i - h_j(x)), \tag{5}$$

where a_i is the average radius for the particles of size range i, and $N_p(x)$ is the number of tracer particles partially overlapping the bin centred about x. The length of the overlapping particle segment $h_j(x)$, is defined in figure 4(*a*). Complete bin overlap was restricted to the large particles, where only one bin could be completely overlapped by a single particle. The tracer particle volume within the completely overlapped bin was calculated from the difference of the average dimensionless volume of the larger tracer particles V_l, and the partial overlap volumes in the two adjacent bins. Generalizing this result for the $N_c(x)$ tracers that completely overlapped the bin centred at x,

$$\begin{array}{l}\text{volume of large}\\ \text{tracer particles due}\\ \text{to complete overlap}\\ \text{of the bin}\\ \text{centred at } x\end{array} = \sum_{j=1}^{N_c(x)} V_l - \frac{\pi}{3}[h_1^2(x-\delta)\,(3a_l - h_j(x-\delta)) + h_j^2(x+\delta)\,(3a_l - h_j(x+\delta))]. \tag{6}$$

As is shown in figure 4(*b*), $h_j(x-\delta)$ and $h_j(x+\delta)$ are the segment lengths for large tracer particle j in the bins adjacent to the one centred about x.

Equations (3)–(6) were used to compute the relative concentration of large and small particles within each of the ten bins. Values for V_s and V_l were calculated assuming that the particles were ideal spheres with respective average particle radii a_s and a_l that were determined from the particle size analysis of §2.1. Values for $h_j(x)$ were computed by subtracting the position of the bin boundary from the experimentally measured tracer particle centre. The uncertainty in the tracer particle volume was also computed by propagating the error associated with measuring a tracer particle position (i.e. $h_j(x)$), and the standard deviation in the distribution data for the two ranges of particle size. This former source was estimated to be $\sqrt{2}a_s \tan\theta_a/\tan\theta_s$ (Lyon 1997). The error associated with each volume calculation given by (4)–(6) was ultimately computed using the general propagation equation

$$e_F = \sum_{i=1}^{N} \left(\frac{\partial F}{\partial x_i}\right)^2 e_i^2, \tag{7}$$

where e_F is the absolute error in the function $F = F(x_i)$, and e_i are the respective uncertainties in the independent variables x_i.

Finally, the relative particle concentration data were converted to absolute volume fractions by satisfying the total flux of particles for each respective size range across the portion of the channel gap over which the bins extend. Using the fact that the flux of particles of each size can be calculated from the case of a uniform concentration

distribution and parabolic velocity profile, the volume fraction of particle size i within the bin centred about x can be written as

$$\phi_i(x) = \left[\frac{\phi_{bulk_i} \int_{-1}^{0.056} (1-x^2)\,\mathrm{d}x}{\int_{-1}^{0.056} v(x)\, V_{t_i}(x)\,\mathrm{d}x} \right] V_{t_i}(x). \tag{8}$$

In (8) $v(x)$ is the LDV measured particle velocity profile across the channel gap, and ϕ_{bulk_i} is the bulk (or mixed) concentration of particles of size range i prescribed for the particular experiment.

4. Results and discussion

The goal of this work was to measure particle velocity and concentration profiles for suspensions possessing a bidisperse particle size distribution undergoing approximate two-dimensional pressure-driven channel flow. Of particular interest was the flow behaviour of the large and small particles as a function of the overall bulk particle concentration ϕ_{bulk}, and the fraction of the total particle volume occupied by small particles x_s, in the mixed suspension. In order to carry out this investigation, the six pairs of LDV/tracer particle experiments listed in table 1 were conducted. For all these experiments the size ratio of the large and small particles a_l/a_s, was fixed at 3.4, which was calculated using the distributions presented in §2.1. Also, to ensure that inertia effects on the measured particle velocity and concentration distributions were negligible, the particle Reynolds number for channel flow defined in Part 1,

$$Re_p \equiv \frac{4}{3}\frac{\rho}{\mu}\frac{\langle a\rangle^3}{H^2} V_{max} \tag{9}$$

and based upon the concentration-averaged particle size,

$$\langle a\rangle = (1-x_s)\, a_l + x_s\, a_s \tag{10}$$

was no larger than 10^{-5}.

As shown in table 1 the highest bulk particle volume fraction in which experiments were performed was 0.40. Although our LDV method is capable of acquiring overall particle velocity and concentration profiles at higher bulk particle loadings (see Part 1), our visual tracer particle experiments were limited to this volume fraction by the inherent turbidity of our index-of-refraction-matched suspensions. This is illustrated by the respective small- and large-tracer-particle photomicrographs presented in figures 5 and 6, which were taken for ϕ_{bulk} and x_s values of 0.40 and 0.75 respectively (i.e. the largest total number of suspended particles investigated). As can be seen in part (*a*) of each figure, tracer particles located roughly $H/4$ from the channel wall can be brought into sharp focus, which enables precise measurement of their position. However, part (*b*) in each figure shows a significant reduction in sharpness for tracer particles that are located in the bin on the opposite side of the channel axis. Tracer particle images at higher particle loadings were even more blurred, which hindered our ability to locate and precisely determine their position. As a result of this optical turbidity, we could not confidently report individual particle concentration profiles for $\phi_{bulk} > 0.40$.

4.1. *Conditions for fully developed velocity and concentration profiles*

As was discussed in Part 1, there exists a total strain for pressure-driven channel flow of concentrated suspensions at which the coupled velocity and concentration profiles

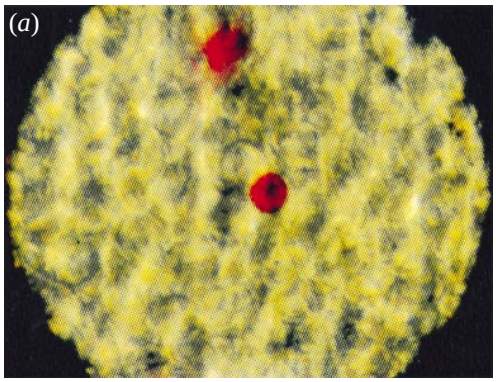

FIGURE 5

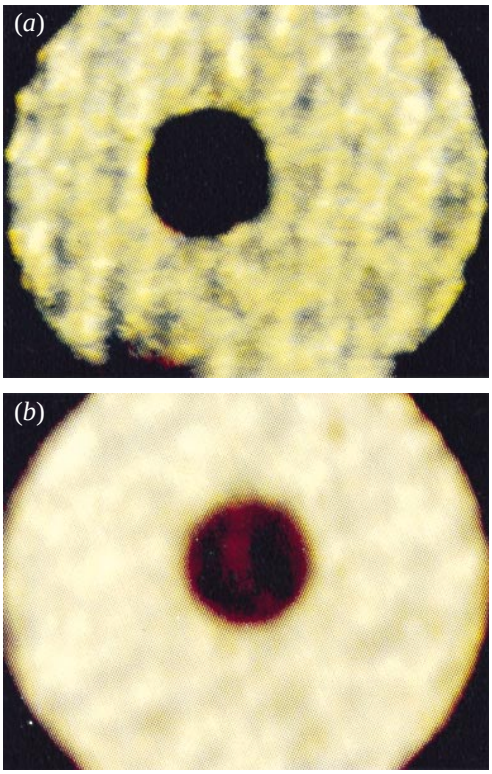

FIGURE 6

FIGURE 5. Photographs of small tracer particles within the index-of-refraction-matched suspension at $\phi_{bulk} = 0.40$ and $x_s = 0.75$. Measured particle positions are (*a*) $x = -0.47$, (*b*) $x = 0.10$.

FIGURE 6. Photographs of larger tracer particles within the index-of-refraction-matched suspension at $\phi_{bulk} = 0.40$ and $x_s = 0.75$. Measured particle positions are (*a*) $x = -0.53$, (*b*) $x = 0.05$.

LDV experiment	Tracer particle experiment	ϕ_{bulk}	x_s	$\langle a \rangle$ (μm)	$H/\langle a \rangle$	Re_p ($\times 10^{-6}$)	$[L/H]_{ss}$	$[L/H]_{exp}$
11	1	0.40	0.25	63.8	14	12.0	18	230
13	2	0.40	0.50	50.0	17	5.6	25	230
17	3	0.40	0.75	36.1	24	2.1	50	230
18	4	0.30	0.75	36.1	24	2.1	200	230
14	5	0.30	0.50	50.0	17	5.6	100	230
15	6	0.30	0.25	63.8	14	12.0	71	230

TABLE 1. List of experimental parameters. The last two columns are the scaling-based relative downstream channel positions required for the measurement of fully developed profiles and the actual experimental values, respectively.

reach fully developed forms that are unchanged by further strain. For convenience, this total strain can be represented by an average dimensionless distance $[L/H]_{ss}$ that a given material volume of suspension must travel down the channel. For monodisperse suspensions $[L/H]_{ss}$ is proportional to the square of the relative width of the channel

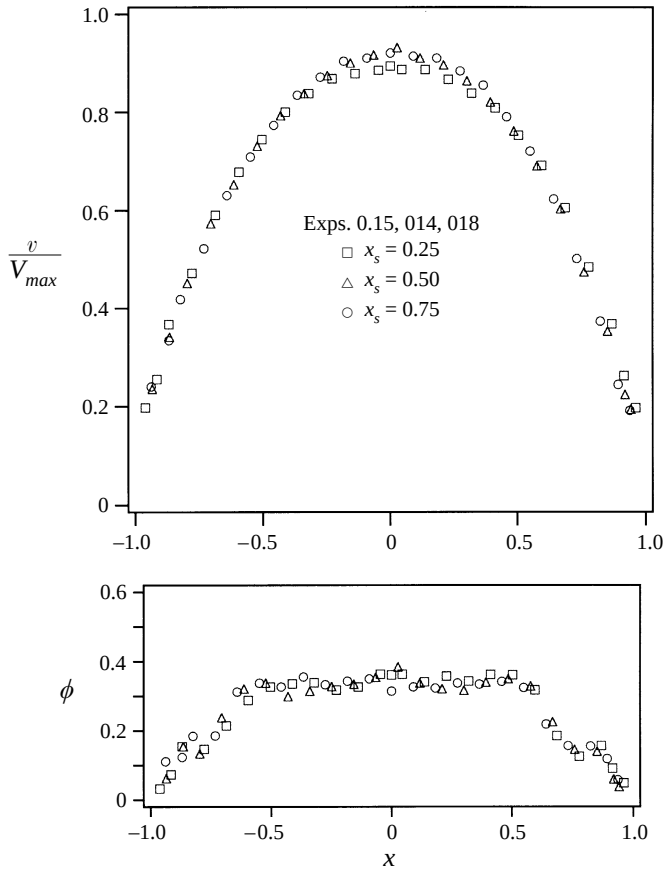

FIGURE 7. Bidisperse suspension LDV velocity and concentration profiles at $\phi_{bulk} = 0.30$.

gap, H/a, and inversely proportional to the dimensionless shear-induced migration coefficient of diffusion, $f(\phi)$ (Nott & Brady 1994),

$$\left[\frac{L}{H}\right]_{ss} \sim \frac{1}{12f(\phi)}\left(\frac{H}{a}\right)^2. \tag{11}$$

This same relationship has been applied to the bidisperse suspensions of interest in this study, where the particle size was approximated by $\langle a \rangle$. The shear-induced coefficient of diffusion $f(\phi)$, was estimated utilizing the empirical formula of Leighton (1985).

$$f(\phi) = \tfrac{1}{3}\phi^2(1 + \tfrac{1}{2}e^{8.8\phi}). \tag{12}$$

Reductions in $f(\phi)$ due to enhancement of the maximum packing fraction of particles for bidisperse systems (Krishnan & Leighton 1995*a*) were neglected, since (12) provided a more conservative estimate for $[L/H]_{ss}$.

Calculated results for $[L/H]_{ss}$ are presented in table 1 along with the dimensionless downstream position $[L/H]_{exp}$, at which the LDA and tracer particle experiments were conducted. Since the dimensionless downstream measuring position is at least six times the calculated induction lengths at $\phi_{bulk} = 0.40$, we believe fully developed velocity and concentration profiles were measured at that particle concentration. For experiments at $\phi_{bulk} = 0.30$, the results of table 1 suggest that fully developed concentration profiles

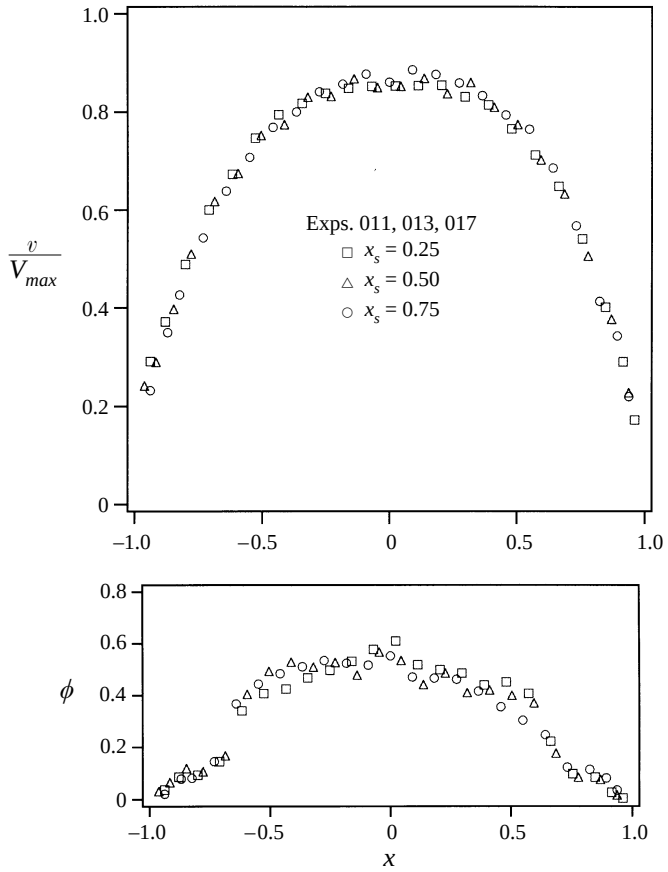

FIGURE 8. Bidisperse suspension LDV velocity and concentration profiles at $\phi_{bulk} = 0.40$.

were clearly measured for $x_s = 0.25$, and were likely to be close to the fully developed state for the other two cases, i.e. $x_s = 0.50$ and 0.75. This is corroborated, in part, by the fact that the overall velocity and concentration profiles measured using LDV were found to be the same for all three of the cases involving $\phi_{bulk} = 0.30$ (see §4.2), in spite of the fact that the ratio $[L/H]_{exp}/[L/H]_{ss}$ ranges from 1.15 to more than 3. A final, definitive conclusion must await additional experimental measurements at even larger values of $[L/H]_{exp}$.

4.2. *LDV velocity and concentrations profiles*

Overall particle velocity and concentration profiles for the three investigated values of x_s are presented in figures 7 and 8 for ϕ_{bulk} values of 0.30 and 0.40, respectively. To facilitate comparisons, error bars representing the standard deviation in the velocity data at each channel gap position have been omitted from the plots. As can be seen by comparing the data at each value of x_s, an increase in ϕ_{bulk} produces a larger concentration of particles within the central region of the channel and a more blunted velocity profile. This same qualitative dependence of the fully developed profiles on ϕ_{bulk} was also reported in Part 1 for suspensions possessing a near monodisperse distribution of particle size. The primary difference from this earlier work is that the overall concentration profiles for $\phi_{bulk} = 0.3$ are somewhat flatter than the corresponding profiles for the monodisperse suspensions at the same bulk particle concentration.

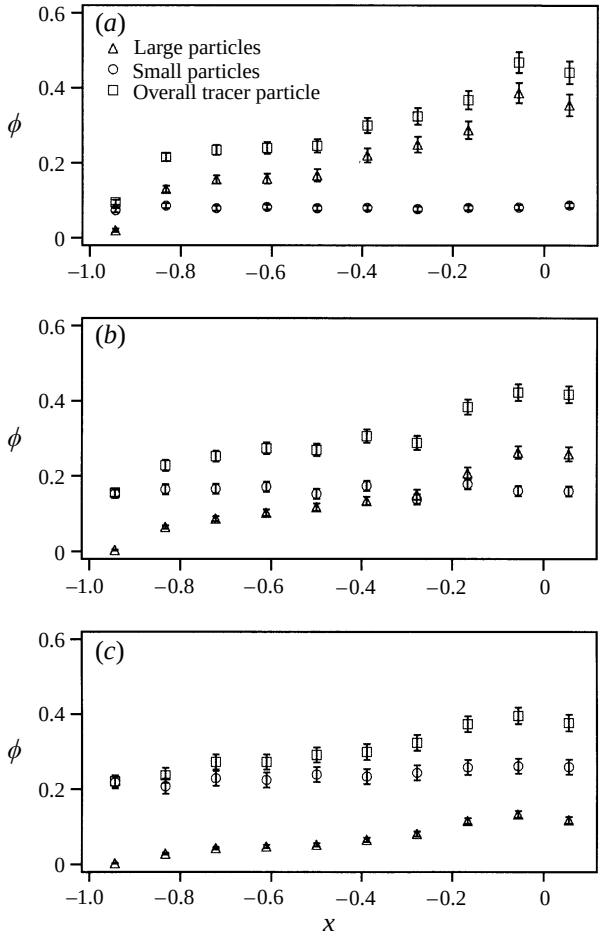

FIGURE 9. Bidisperse suspension tracer-particle concentration profiles at $\phi_{bulk} = 0.30$: (*a*) $x_s = 0.25$, (*b*) $x_s = 0.50$, (*c*) $x_s = 0.75$.

The lack of any measurable influence of x_s on the overall velocity and concentration profiles is also evident in figures 7 and 8. At each value of ϕ_{bulk} the velocity and concentration distributions were identical, within experimental uncertainty, over the range of x_s that was investigated. This is consistent with the statistically indistinguishable distributions reported in Part 1 for monodisperse suspensions in the range $11 \leqslant H/a \leqslant 24$. That is, when each bidisperse suspension is considered as an equivalent monodisperse system with concentration-averaged particle size $\langle a \rangle$, the bidisperse velocity and concentration profiles represent a similar range of equivalent relative channel gap width $14 \leqslant H/\langle a \rangle \leqslant 24$. As suggested earlier, it is also an indication that the profiles for $\phi_{bulk} = 0.3$ are very nearly fully developed. If this were not the case, one would expect to see different profiles for each value of x_s, since there is a significant change in $[L/H]_{ss}$ with x_s (see table 1). It is noteworthy to add that one of the profiles for $\phi_{bulk} = 0.3$ has very nearly the same value of $[L/H]_{ss}$ as the case $\phi_{bulk} = 0.4$ and $x_s = 0.75$. The difference in the shapes of the concentration profiles for $\phi_{bulk} = 0.3$ and $\phi_{bulk} = 0.4$ is presumed to be a reflection of true fully developed states being measured in each case. While it is unclear why the profile for $\phi_{bulk} = 0.3$ should be flatter than the profiles at $\phi_{bulk} = 0.4$, or for a monodisperse suspension at $\phi_{bulk} = 0.3$, there is also no reason to suppose that those profiles should be the same.

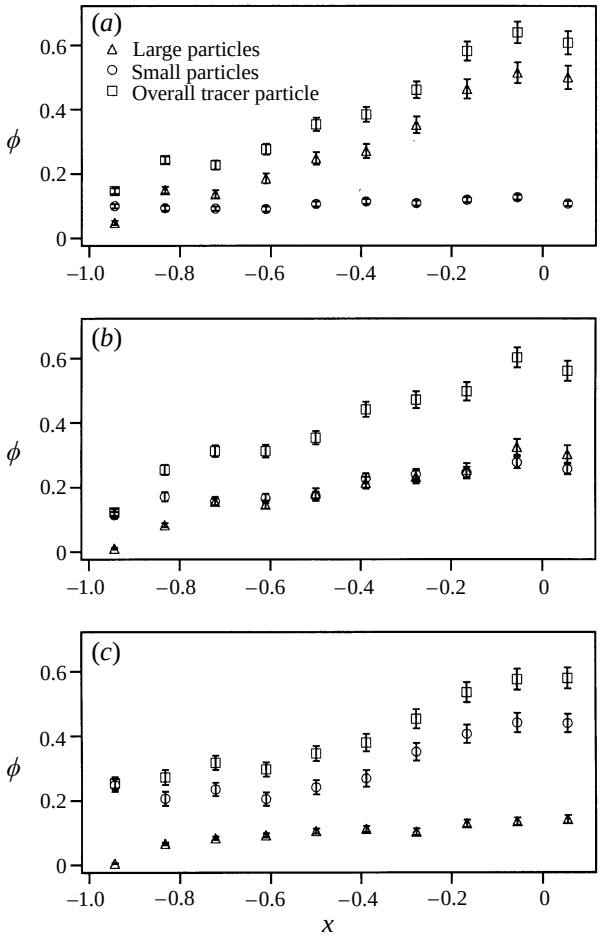

FIGURE 10. Bidisperse suspension tracer-particle concentration profiles at $\phi_{bulk} = 0.40$: (*a*) $c_s = 0.25$, (*b*) $x_s = 0.50$, (*c*) $x_s = 0.75$.

4.3. *Tracer-particle concentration profiles*

Individual concentration profiles for the large and small particles are presented as a function of x_s for bulk particle concentrations of 0.30 and 0.40 in figures 9 and 10, respectively. Also shown are the overall concentration distributions, obtained by summing the results for the large and small particles at each spatial position (i.e. bin). These will be compared with the LDV results of figures 7 and 8 shortly.

The individual particle size concentration profiles shown in figures 9 and 10 reveal different behaviours for the large and small particles. In all cases, the distribution of large particles across the channel gap was non-uniform with a maximum in the region near the channel axis and a minimum near the wall. Results for the small particles, on the other hand, depended upon both x_s and ϕ_{bulk}. For $\phi_{bulk} = 0.40$, the small-particle profiles were uniform for the smallest relative concentration, $x_s = 0.25$, but became increasingly non-uniform for $x_s = 0.50$ and 0.75. On the other hand, for $\phi_{bulk} = 0.30$, the small-particle profiles were essentially uniform for all three values of x_s. Although we have argued that the overall concentration and velocity profiles are suggestive of the fact that the profiles for $\phi_{bulk} = 0.30$ are 'fully developed', it is possible that the uniform small-particle profiles for the largest two values of x_s are partly due to the fact

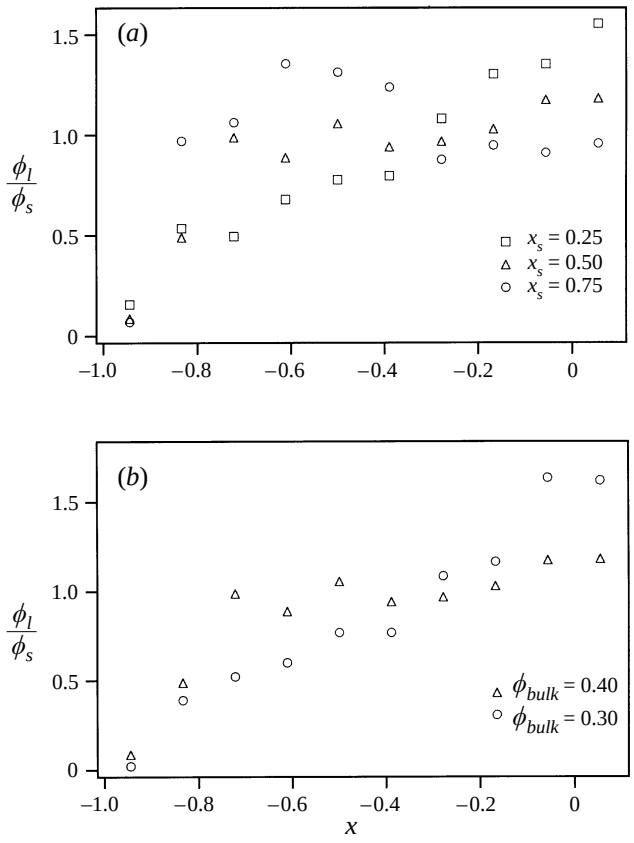

FIGURE 11. The influence of (*a*) x_s and (*b*) ϕ_{bulk} on flow-induced size segregation of the suspended particles. The data in (*a*) are at $\phi_{bulk} = 0.40$, while the data in (*b*) correspond to $x_s = 0.50$. The data suggest that the enrichment of large particles in the axis region of the channel increases as either x_s or ϕ_{bulk} decreases.

that $[L/H]_{exp}/[L/H]_{ss} \leqslant O(2)$ is not quite large enough. It is, for example, possible that the overall concentration profile reaches a fully developed state quite quickly, while there remains some adjustment (or evolution) for the individual large- and small-particle profiles. There is no way to definitively prove whether this is a factor short of experiments in a longer channel. However, we believe that the case $x_s = 0.25$, where $[L/H]_{exp}/[L/H]_{ss} > 3$ is most certainly in a fully developed state, as well as all of the results for $\phi_{bulk} = 0.40$.

The presence of uniform (or more uniform) concentration distributions for the small suspended microspheres, and non-uniform profiles for the large particles strongly reflect flow-induced size segregation. That is, the fraction of large particles in the suspension is greater near the centre of the channel than in the bulk. A similar large-particle enrichment phenomenon has been reported for other two dimensional flows (Abbott *et al.* 1991; Husband *et al.* 1994; Krishnan & Leighton 1994; Chow *et al.* 1995), and is consistent with the particle size dependence of the migration velocity of the diffusive flux model (Leighton & Acrivos 1987; Phillips *et al.* 1992).

To quantify the influence of the relative concentration of large particles within the bulk suspension on particle size segregation, the concentration ratio of large to small particles within each bin ϕ_l/ϕ_s, was calculated from the measured concentration

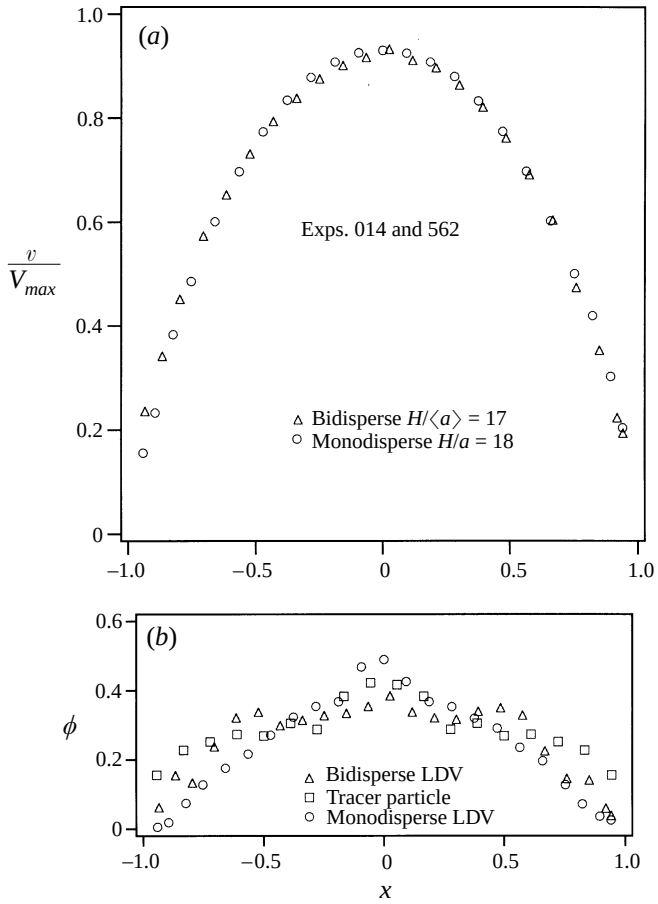

FIGURE 12. Comparison of (*a*) LDV bidisperse and monodisperse velocity profiles results, and (*b*) LDV bidisperse, LDV monodisperse, and overall tracer-particle concentration profile data, for $\phi_{bulk} = 0.30$, and a relative channel gap width of 14 particle diameters.

profiles at $\phi_{bulk} = 0.40$ and normalized by the known value (i.e. x_s) in the mixed suspension. Results presented in figure 11(*a*) show that the relative concentration of large particles in the region away from the channel walls increases as the overall fraction of large particles in the suspension is increased. Conversely, a larger volume fraction of small particles is found near the centre of the channel when $x_s = 0.75$. The influence of the overall bulk particle concentration, ϕ_{bulk}, on particle enrichment can also be determined by comparing results for $\phi_{bulk} = 0.30$ and 0.40 (assuming of course, that the profiles for $\phi_{bulk} = 0.30$ are fully developed). In figure 11(*b*) we present ϕ_l/ϕ_s within each bin from the large- and small-particle concentration distributions for the case $x_s = 0.50$ from figures 9 and 10. As is shown, larger ϕ_l/ϕ_s values in the central region of the channel result at $\phi_{bulk} = 0.30$, which suggests that size segregation is enhanced with decreasing ϕ_{bulk}. Similar results for the effects of ϕ_{bulk} and the relative concentration of large particles in the mixed suspension have also been reported for concentrated suspension flows behind an advancing meniscus (Chow *et al.* 1995), and at the air-suspension surface of an open channel flow (Husband *et al.* 1994). Like these other investigators, we believe these effects are a consequence of enhanced particle screening due to an increase in the total number of suspended particles.

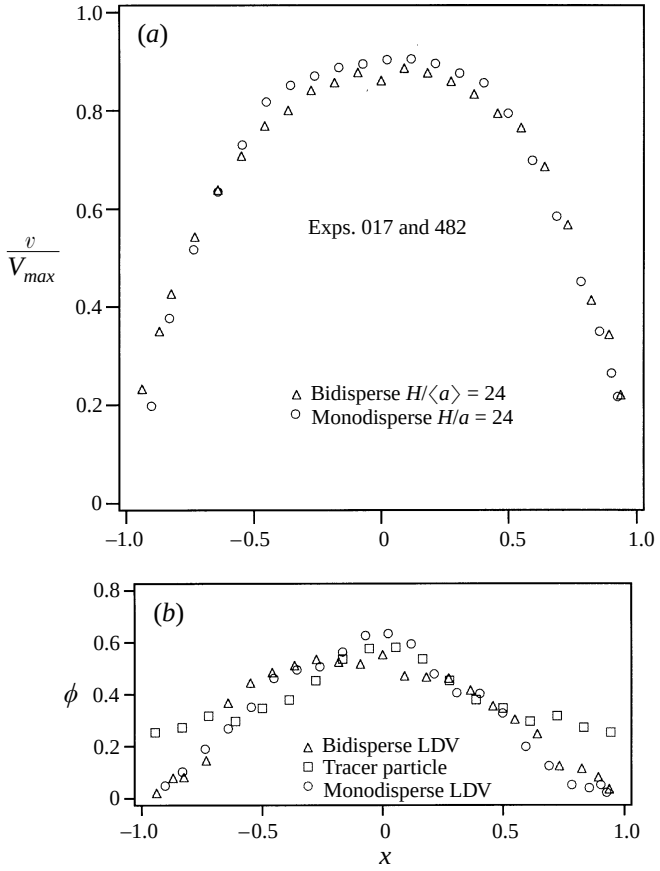

FIGURE 13. As figure 12 but for $\phi_{bulk} = 0.40$, and a relative channel gap width of 24 particle diameters.

4.4. *Comparisons with monodisperse LDV data*

Comparisons of the bidisperse LDV, overall tracer particle, and monodisperse LDV data from Part 1 are presented in figures 12 and 13. In figure 12 we consider $\phi_{bulk} = 0.30$, with $H/a = 18$ for the monodisperse suspension and $H/\langle a\rangle = 17$ for the bidisperse system. Figure 13 contains the data at $\phi_{bulk} = 0.40$ and H/a (or $H/\langle a\rangle$) equal to 24. Similar results were also found for the other four sets of corresponding monodisperse and bidisperse data. Note that the tracer-particle concentration values for $x \geqslant 0.06$ are reproduced from the data on the opposite side of the channel symmetry axis. In part (*b*) of each figure qualitative agreement between the three sets of concentration data is evident; however, a distinct difference is also observed. First, the tracer particle concentration values tend to be larger than both LDV results in the outer 20% of the channel gap. As stated in Part 1, we suspect that the intrinsic inaccuracy of the LDV method in the region near the wall is partially responsible for this difference. Inherent to LDV is a lower signal-to-noise ratio near flow boundaries. With regard to particle concentration measurements, this lower signal-to-noise ratio produces larger average times between consecutive Doppler bursts, and an apparent lower particle concentration. As was noted in Part 1, this difference increases with corresponding increases in ϕ_{bulk} and $H/\langle a\rangle$ (or H/a), and has led us to conclude that

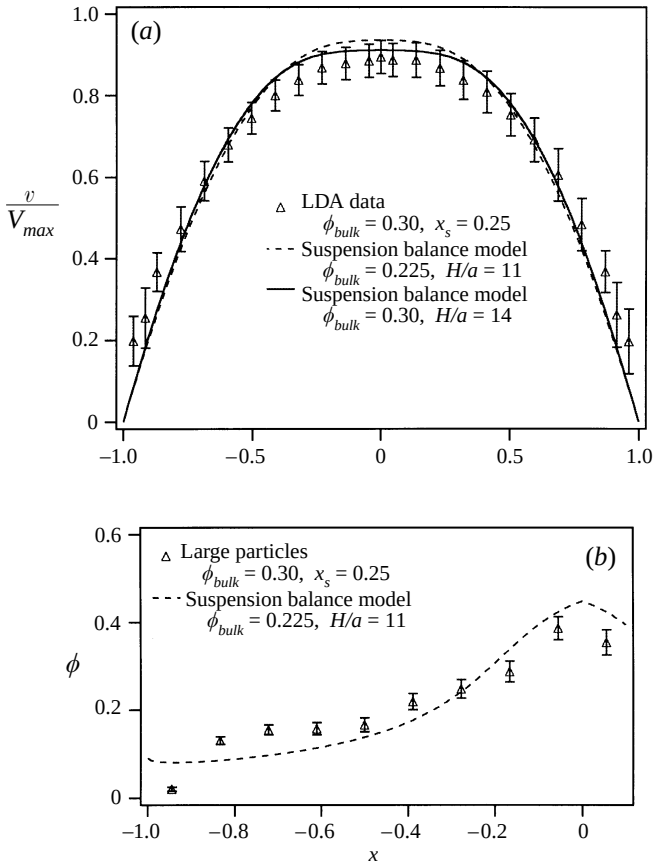

FIGURE 14. Comparison of suspension balance model velocity and concentration profile calculations at $\phi_{bulk} = 0.225$ and $H/a = 11$ with bidisperse LDV velocity and large-tracer particle concentration data at $Re_p = 1.2 \times 10^{-5}$, $\phi_{bulk} = 0.30$, and $x_s = 0.25$. Velocity profile results for suspension balance model calculations at $\phi_{bulk} = 0.30$ and $H/a = 11$ are included since this provides a better fit to the experimental velocity data.

we cannot confidently report LDV concentration profile data at points lying in the outer 20% of the channel gap.

In figures 12(*a*) and 13(*a*) the LDV velocity profiles for the bidisperse and monodisperse suspensions are presented. As can be seen in both figures, the velocity profiles for each suspension are the same, within experimental uncertainty. We believe that this result is a consequence of the relatively weak coupling that exists between the particle velocity and concentration profiles. That is, the small quantitative differences in the monodisperse and bidisperse concentration distribution (other than the LDV data near the walls) shown in the part (*b*) of each figure cannot be discerned in the corresponding velocity profiles.

4.5. *Suspension balance model comparisons*

The observation of uniform small-particle concentration distributions at $x_s = 0.25$ for the two values of bulk particle concentration probed suggests that these suspension flows could be treated theoretically as monodisperse systems whose flow properties are determined only from the distribution of large particles. That is, the uniform viscosity contribution of the small particles within the gap enables the suspension to be

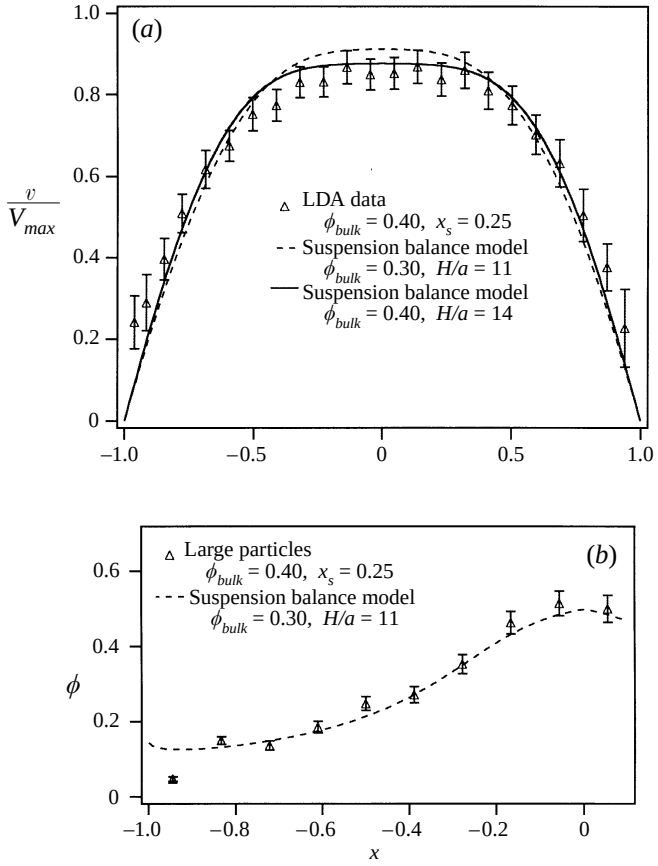

FIGURE 15. Comparison of suspension balance model velocity and concentration profile calculations at $\phi_{bulk} = 0.30$ and $H/a = 11$ with bidisperse LDV velocity and large-tracer particle concentration data at $Re_p = 1.2 \times 10^{-5}$, $\phi_{bulk} = 0.40$, and $x_s = 0.25$. Velocity profile results for suspension balance model calculations at $\phi_{bulk} = 0.40$ and $H/a = 11$ are included since this provides a better fit to the experimental velocity data.

envisaged as a less concentrated monodisperse system consisting of the large particles immersed in an effective suspending medium. Similar monodisperse behaviour has also been reported at $x_s = 0.25$ for measurement of the large–large particle pair distribution function by Krishnan & Leighton (1995*b*). This apparent lack of small-particle influence motivated us to compare the measured large-particle distributions at $x_s = 0.25$ with suspension balance model predictions at a relative channel gap width that corresponded to the average large-particle radius (i.e. $H/a = 11$), and bulk particle concentrations equal to that of the large particles. Since the best fit version of the suspension balance model (McTigue & Jenkins 1992; Nott & Brady 1994) discussed in Part 1 provided a close agreement with the experimental monodisperse LDV data, it was used for these comparisons.

Experimental results for the overall particle velocity and large-particle concentration profiles are presented in figures 14 and 15 for the experiments at $x_s = 0.25$ and respective bulk particle concentrations of 0.30 and 0.40. Also included in each plot are suspension balance model predictions in which the suspension is treated as a monodisperse system consisting only of the large particles at the actual large-particle concentration and size ($H/a = 11$). Model velocity predictions in which the suspension

is treated as monodisperse, but consisting of particles whose concentration-average size is given by (10) (i.e. $H/a = 14$ in the model calculations), and whose concentration is the overall value are shown in the part (*a*) of each figure. As can be seen in the bottom plot of each figure, the agreement between model predictions and the large-tracer-particle concentration profiles is reasonable, particularly for the experimental data at $\phi_{bulk} = 0.40$. However, a poor fit is provided by the model velocity profile when the suspension is treated as a monodisperse system consisting only of the large particles. In fact, a better fit to the experimental velocity data is found when the entire suspension concentration and the average particle size are utilized. These results suggest that although the small-particle distribution is uniform, their presence influences the flow to a greater extent than by simply providing an incremental increase in background viscosity to the suspending liquid. The small particles also bring the overall particle concentration closer to the maximum packing fraction, where the suspension viscosity is more sensitive to particle concentration. Within this more sensitive regime, variations in the local particle concentration produce larger variations in the local viscosity, which results in a more blunted velocity profile.

5. Summary

In this work we have applied our modified laser Doppler velocimetry technique to obtain overall particle velocity and concentration profiles for suspensions possessing a bidisperse of particle size under Poiseuille flow conditions. These results were augmented by concentration distribution measurements for the suspended particles of each size range, which were obtained by sampling tracer particle positions across 60 % of the narrow channel gap. Non-uniform overall concentration distributions and modified velocity profiles were measured, and quantitative data were presented for particle size segregation as a function of overall bulk particle concentration and the fraction of the bulk composed of small particles.

As noted in the monodisperse work described in Part 1, it would be interesting in a future investigation of bidisperse systems to study the evolution of the particle velocity and concentration profiles as a function of downstream measuring position. Obviously, such a study would be extremely valuable in the development of a model that is capable of accounting for particle size segregation as well as the development of non-uniform particle-phase concentration profiles. The results of the work presented here suggest that in order for such a model to provide accurate predictions of the suspended particle velocity profile, it must account for the presence of the small particles regardless of their distribution within the conduit cross-section.

REFERENCES

Abbot, J. R., Tetlow, N. 1991 Experimental observations of particle migration in concentrated suspensions: Couette flow. *J. Rheol.* **35**, 773–795.

Beyer, W. H. 1984 *Standard Mathematical Tables*. CRC Press Inc.

Chang, C. & Powell, R. L. 1994 Effect of particle size distributions on the rheology of concentrated bimodal suspensions. *J. Rheol.* **38**, 85–98.

Chong, J. S., Christiansen, E. B. 1971 Rheology of concentrated suspensions. *J. Appl. Polymer Sci.* **15**, 2007–2021.

Chow, A. W., Hamlin, R. D. 1995 Size segregation of concentrated, bidisperse and polydisperse suspensions during tube drawing. *IUTAM Symp. on Hydrodynamic Diffusion of Suspended Particles, Estes Park, CO*.

GRAHAM, A. L., ALTOBELLI, S. A. 1991 NMR imaging of shear-induced diffusion and structure in concentrated suspensions. *J. Rheol.* **35**, 191–201.

HAMPTON, R. E., MAMMOLI, A. A. 1996 Migration of particles undergoing pressure driven flow in a circular conduit. *J. Rheol.* **41**, 621–640.

HUSBAND, D. M., MONDY, L. A. 1994 Direct measurements of shear-induced particle migration in suspensions of bimodal spheres. *Rheol. Acta* **33**, 185–192.

KRISHNAN, G. P., BEIMFOHR, S. 1996 Shear-induced radial segregation in bidisperse suspensions. *J. Fluid Mech.* **321**, 371–393.

KRISHNAN, G. P. & LEIGHTON, D. T. 1995*a* Dynamic viscous resuspension of bidisperse suspensions I. Effective diffusivity. *Int J. Multiphase Flow* **21**, 721–732.

KRISHNAM, G. P. & LEIGHTON, D. T. 1995*b* Shear-induced structure in bidisperse suspensions. *IUTAM Symp. on Hydrodynamic Diffusion of Suspended Particles*, *Estes Park*, *CO*.

KRISHNAN, G. P. & LEIGHTON JR D. T. 1994 Shear-induced size segregation phenomena in bidisperse suspensions. In *Mechanics USA 1994*. Applied Mechanics Review, ASME.

LEIGHTON, D. T. 1985 The shear induced migration of particulates in concentrated suspensions. PhD, thesis, Stanford University.

LEIGHTON, D. & ACRIVOS, A. 1987 The shear-induced migration of particles in concentrated suspensions. *J. Fluid Mech.* **181**, 415–439.

LYON, M. K. 1997 Experimental studies of noncolloidal suspensions undergoing two-dimensional flow. PhD thesis, University of California, Santa Barbara.

LYON, M. K. & LEAL, L. G. 1998 An experimental study of the motion of concentrated suspensions in two-dimensional channel flow. Part 1. Monodisperse systems. *J. Fluid Mech.* **363**, 25–56.

MCTIGUE, D. F. & JENKINS, J. T. 1992 Channel flow of a concentrated suspension. In *Advances in Micromechanics of Granular Materials* (ed. H. H. Shen, M. Satake, M. Mehrabadi, C. S. Chang & C. S. Campbell), pp. 381–481. Elsevier.

NOTT, P. R. & BRADY, J. F. 1994 Pressure-driven flow of suspensions: stimulation and theory. *J. Fluid Mech.* **275**, 157–199.

PHAN-THIEN, N. & FANG, Z. 1996 Entrance length and pulsatile flows of a model concentrated suspension. *J. Rheol.* **40**, 521–529.

PHILLIPS, R. J., ARMSTRONG, R. C. 1992 A constitutive equation for concentrated suspensions that accounts for shear-induced particle migration. *Phys. Fluids* A **4**, 30–39.

STORMS, R. F., RAMARAO, B. V. 1990 Low shear rate viscosity of bimodally dispersed suspensions. *Powder Technol.* **63**, 247–259.